methyltransferase, is recruited through TAD2.[21–24] Sumegi *et al.*[12] demonstrated that deletion of TAD1 from PAX3-NCOA2 more strongly suppressed the transforming activity of the chimeric protein than did deletion of TAD2, and PAX3-NCOA2 needed an intact activation domain 2(TAD2) and CID for optimal transforming activity using the NIH3T3 mouse fibroblast cell line. Both TADs on NCOA2 boost transcriptional activation of PAX3-NCOA2, as they do in PAX3-FOXO1A.

However, the role of the *NCOA2* rearrangement including *PAX3-NCOA2* in RMS tumorigenesis remains to be elucidated. In this study, we compared the biological function of the *PAX3-NCOA2* fusion protein with *PAX3-FOXO1A* fusion protein to reveal the function of PAX3-NCOA2 in RMS tumorigenesis both *in vitro* and *in vivo*. To this end, we expressed these two fusion genes in C2C12 mouse myoblast cell lines and studied their biological character.

RESULTS

PAX3-NCOA2 was identified in an ERMS tumor specimen and transcriptional activation of the PAX3 consensus-binding site was enhanced

We previously showed the *PAX3* rearrangement in our case with ERMS by FISH analysis.[13] To identify the partner gene of *PAX3* in this case with the complex translocation involving 2q35 and 8q13, and so on, we narrowed down the 8q13 breakpoint region by stepwise FISH approach using bacterial artificial chromosome (BAC) probes located on chromosome 8q13. The results demonstrated that the BAC clone RP11-479K21 (located at 8q13.3) spanned the 8q13 breakpoint, and that the split signal of RP11-479K21 probe was fused to the signal of RP11-624P23 (on the telomeric side of the *PAX3* gene located at 2q35) (data not shown). RP11-479K21 clone contained the *NCOA2* gene. These results suggested that the candidate partner gene of *PAX3* was *NCOA2* in our case with ERMS. Sequence analysis of the *PAX3-NCOA2* PCR products of our patient's sample revealed that exon 7 of *PAX3* (391st AA) was fused to exon 12 (798th AA) of the *NCOA2* gene in-frame (Figure 1a). The resulting *PAX3-NCOA2* fusion protein consisted of the 391 N-terminal AA of PAX3 and the 666 C-terminal AA of NCOA2. A schema of the structures of intact and chimeric proteins is shown in Figure 1b. The *PAX3-NCOA2* fusion gene retained the DNA-binding domain of PAX3, and the CID/TAD1 and TAD2 domains of NCOA2, in agreement with the findings of Sumegi *et al.*[12] When HEK293 cells were transfected with the GFP-PAX3-NCOA2 expression vector, PAX3-NCOA2 localized in the nucleus (Figures 2a and b). The expressions of PAX3-NCOA2 enhanced transcriptional activation of the PAX3 consensus-binding site 3.8 times more than did the expression of the wild-type PAX3 and the expression of PAX3-FOXO1A enhanced it 19.8 times more (both $P<0.05$) (Figure 2c).

PAX3-NCOA2 stimulated proliferation and motility in myoblasts *in vitro*

We confirmed the protein expressions of PAX3-NCOA2 and PAX3-FOXO1A in HEK293 cells transiently transfected with FLAG-tagged constructs by western blotting (Figure 3a). Cell proliferation was assessed using C2C12 cells expressing PAX3-NCOA2, PAX3-FOXO1A or MSCV empty vector. On day 4, the numbers of PAX3-NCOA2 C2C12 cells and PAX3-FOXO1A C2C12 cells were 1.3 times more ($P<0.05$) and 1.7 times more ($P<0.05$), respectively, than the number of control cells (Figure 3b). The PAX3-NCOA2 cells switched from the G1phase to the S phase and showed an accelerated cell cycle progression (Figure 3c). Wound closure was more rapid with both the PAX3-NCOA2 cells and PAX3-FOXO1A cells than with the control cells (Figure 3d), indicating that the transformed cells have an enhanced motility. However, the wound width (% of original width) indicated that the PAX3-NCOA2 cells were not as motile as the PAX3-FOXO1A cells. When the cells were plated on soft agar, 3 ± 0.5 colonies grew from the control cells, whereas 53.6 ± 4.2 and 115.2 ± 0.5 colonies grew from the PAX3-NCOA2 cells and PAX3-FOXO1A cells (Figure 3f), respectively, indicating that both lines were capable of anchorage-independent growth. However, anchorage-independent growth of the PAX3-NCOA2 cells was only about half that of the PAX3-FOXO1A cells (Figure 3g).

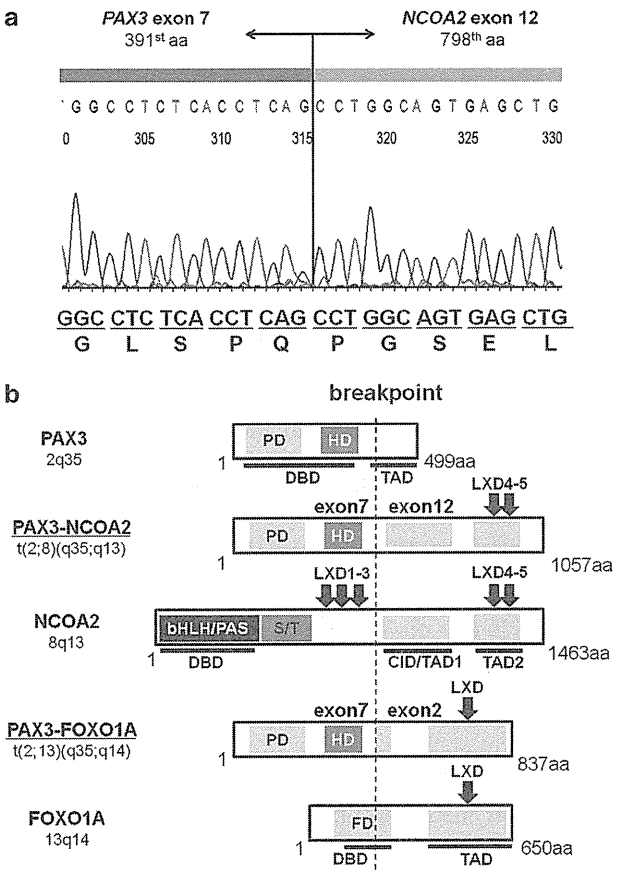

Figure 1. In-frame fusion of exon 7 of *PAX3* to exon 12 of *NCOA2*. (**a**) Representative RT–PCR and sequence analyses for chimeric transcripts in our patient. Sequence alignment of the *PAX3-NCOA2* breakpoint regions. Arrows depict the fusion point. Single-letter amino-acid code is displayed beneath the nucleotide sequence. (**b**) Comparison of wild type, fusion products associated with the t(2;8)(q35; q13) and t(2;13)(q35; q14) translocation. Interacting proteins are displayed as bars. The letters within the bars designate conserved domains (PD, paired domain; HD, homeodomain of the PAX3 protein; CID, CBP interaction domain; and bHLH/PAS, DNA-binding/protein heterodimerization domain, receptor nuclear translocator domain, involved in DNA binding). S/T represents the serine-threonine-rich region. Transcriptional domains of PAX3 are DBD (DNA-binding domain) and TAD (transcriptional activation domain). Arrows show the locations of LXXLL motifs in wild-type NCOA2, FOXO1A and their fusion proteins. NCOA2 has all five motifs, but the three on the N-terminus were lost during formation of PAX3-NCOA2. On the other hand, FOXO1A has only one motif, which is retained in PAX3-FOXO1A. All of the motifs on PAX3-NCOA2 (LXD4-5) and PAX3-FOXO1A (LXD) are in their transactivation domains. LXD, LXXLL-containing helical motif.

PAX3-NCOA2 inhibited the differentiation from myoblasts into myotubes in the differentiation medium

PAX3-NCOA2 and PAX3-FOXO1A morphologically blocked myotube differentiation (Figure 4a). Few of either PAX3-NCOA2

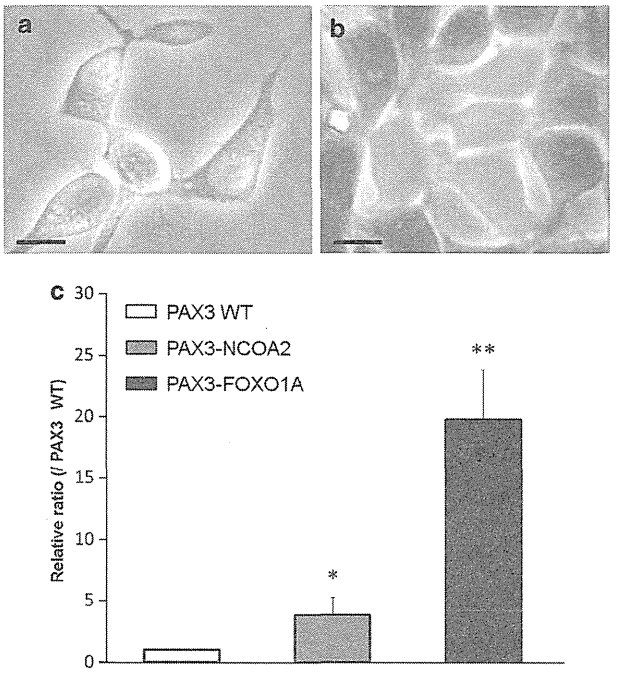

Figure 2. Confocal microscopy images showing localization of PAX3-NCOA2 in HEK293 cells. Cells were transfected with (**a**) GFP-PAX3-NCOA2 expression vector or (**b**) GFP empty vector. Scale bar, 20 μm. (**c**) Expression of PAX3-NCOA2 promoted transcriptional activation of PAX3 consensus-binding site by luciferase assay. Results represent the means ± s.d. of three independent experiments. $^{*}P<0.05$ and $^{**}P<0.01$ compared with wild-type PAX3.

or PAX3-FOXO1A cells were stained with myosin heavy chain (MHC), a marker of muscle differentiation (Figure 4b). MHC positivity of PAX3-NCOA2-expressing cells and PAX3-FOXO1A-expressing cells were 2.3 ± 0.3% and 0.3 ± 0.3%, respectively, whereas the control cells was 53.0 ± 3.8% ($P<0.05$) (Figure 4c).

PAX3-NCOA2 promoted tumorigenesis *in vivo*

When fibroblasts expressing the fusion genes were transplanted into nude mice, the PAX3-NCOA2 and PAX3-FOXO1A cells took ~6.8 and 5.2 weeks, respectively, to form 15-mm-diameter tumors (Figure 5a). Therefore, tumorigenic properties of the PAX3-NCOA2 and PAX3-FOXO1A cell lines well reflect their *in vitro* anchorage-independent growth.

Every tumor was solid, firm and fibrotic. Unexpectedly, the tumors induced by the PAX3-NCOA2 and PAX3-FOXO1A cells did not differ with respect to any of eight characteristics examined: cell shapes, growth pattern/architecture, cellular cohesiveness, muscle differentiation, number of giant cells, nuclear-to-cytoplasm volume ratio reversal, hyperchromatism, cellular/nuclear pleomophism and stromal matrix. None of the tumors displayed the alveolar architectures on H&E stain and silver impregnation (Figure 5b, i–iii). All tumors were generally densely cellular and were mainly composed of a mixture of primitive RMS cells and limited numbers of nucleated giant cells and spindle-shaped tumor cells without myxoid stroma. All tumors stained positive for desmin, myoD1 and myogenin (Figure 5b, iv–vi), which are commonly used markers for RMS. Although some tumors showed evidence of local invasion, none of the tumor-bearing mice developed metastasis.

The LXXLL motifs of PAX3-NCOA2 was not required for anchorage-independent growth

The LXXLL motif (where L is leucine and X is any amino acid) is found in various co-activators, including NCOA[25,26] and FOXO family proteins, as well as in PAX3-NCOA2 and PAX3-FOXO1A (Figure 1b). To examine whether the LXXLL motif is involved in anchorage-independent growth, we constructed mutation/deletion constructs of the motif (Supplementary Table 1) following previous reports.[27,28] However, these mutations and deletions did not significantly affect anchorage-independent growth of either cell line (Figure 6), suggesting that the LXXLL motif is not a promising therapeutic target.

DISCUSSION

Our *in vitro* results revealed that the expression of PAX3-NCOA2 promoted transcriptional activation of the PAX3 consensus-binding site and that PAX3-NCOA2 actually acted as a transcriptional activator. PAX3-NCOA2 also enhanced proliferation, cell cycle progression, motility and anchorage-independent growth. In addition, we showed that PAX3-NCOA2 blocked myotube differentiation. These data indicated that PAX3-NCOA2 has a dual role in the tumorigenesis of RMS: promotion of cell proliferation and inhibition of myogenic differentiation. Our PAX3-NCOA2 results bear a close resemblance to previous findings that PAX3-FOXO1A promoted cell proliferation and motility and inhibited differentiation.[29–31] Our results suggest that PAX3-NCOA2 and PAX3-FOXO1A share the same mechanism for tumorigenesis. Finckenstein *et al.*[32] called *PAX3-FOXO1A* genes 'pangenes' in tumorigenesis, meaning that they simultaneously initiate myogenesis and inhibit terminal differentiation. It is not surprising that *PAX3-NCOA2* acts as a pangene like *PAX3-FOXO1A* because *PAX3-NCOA2* induces tumors derived from muscle tissue *in vivo*.

The tumors in nude mice derived from C2C12 cells transformed with PAX3-NCOA2 share several pathologic features with human ERMS tumor samples: the shapes of cells were small and round or spindle-like, and the cells having abundant cytoplasm were irregularly distributed among immature undifferentiated cells (Figure 5b, i–vi). Although PAX3-FOXO1A-expressing C2C12 cells developed non-invasive ERMS-like tumors in our experiment, Zhang *et al.*[33] showed that mouse myoblasts transformed with PAX3-FOXO1A-induced malignant, ARMS-like tumors in mice. In addition, almost all PAX3-FOXO1A tumor-bearing mice develop spontaneous metastasis to the lungs, one of the targeted sites for metastasis in human ARMS. On the other hand, Wang *et al.*[34] reported that a PAX3-FOXO1A stable cell line formed tumors but the tumors did not have alveolar structure and did not invade any organ, in agreement with our results. As suggested by Naini *et al.*[35], whether or not a tumor is malignant with alveolar structure may depend on not only PAX3-FOXO1A but also one or more other abnormalities as well, loss of p16INK4A/p14ARF or overexpression of MYCN.

Sumegi *et al.*[12] did not report the prognosis of his patients with the *PAX3-NCOA2* fusion gene. However, our case had localized RMS, responded to standard therapy and is alive and in remission at 9 years after treatment. Mosquera *et al.*[11] also reported recurrent *NCOA2* rearrangements in spindle cell-type RMS, which is a subtype with good prognosis. In all of our experiments, the most aggressive phenotype was PAX3-FOXO1A, followed by PAX3-NCOA2, as expected. The finding that the PAX3-NCOA2 stable cell line expressed a less aggressive phenotype than did the PAX3-FOXO1A stable cell line supports our hypothesis that RMS with the *PAX3-NCOA2* fusion gene has a better prognosis than RMS with the *PAX3-FOXO1A* fusion gene.

The LXXLL motif was originally observed in cofactor proteins that interact with hormone-activated nuclear receptors.[25]

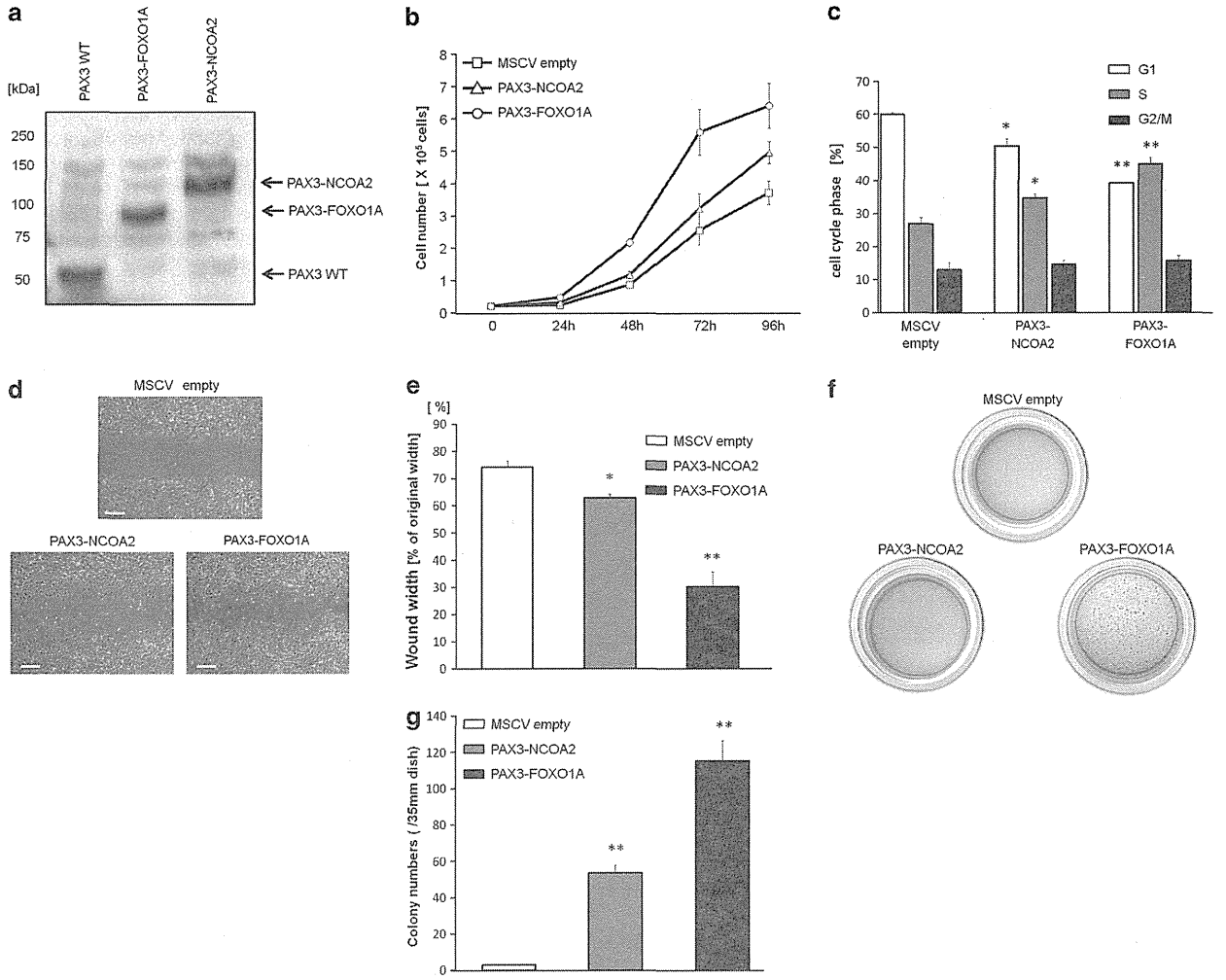

Figure 3. Promotion of some characteristics of tumorigenesis by PAX3-NCOA2. (**a**) Western blot showing expressions of intact and chimeric genes. The molecular weights of wild-type PAX3, PAX3-FOXO1A, and PAX3-NCOA2 were 53, 97 and 120 kDa, respectively. (**b**) Cell growth of C2C12 with and without the chimeric gene 96 h later. Results represent the means ± s.d. from three independent experiments. (**c**) Cell cycle of C2C12 with and without the chimeric gene 72 h later as determined by flow cytometry. Results represent the means ± s.d. of three independent experiments. $^{*}P<0.05$ and $^{**}P<0.01$ compared with the same phase of MSCV empty vector. (**d**) Light microscopic images of C2C12 cells that were scratched using a pipette tip and compared the wound width 6 h later. Scale bar, 100 μm. (**e**) Average wound widths, expressed as a percent of the original width, obtained from 30 measurements in each photo. PAX3-NCOA2 enhances motility of mouse myoblasts. Results represent the means ± s.d. of three independent experiments. $^{*}P<0.05$ and $^{**}P<0.01$ compared with MSCV empty vector. (**f**) Photographs of colonies of C2C12 cells with and without the chimeric gene 14 days later. (**g**) Anchorage-independent growth of the three cell types using a colony-forming soft agar assay as described in Materials and methods. Results represent the means ± s.d. of three independent experiments. $^{**}P<0.01$ compared with MSCV empty vector.

Functionally active examples of LXXLL motifs have also been documented in proteins that do not directly interact with nuclear receptors, including several transcription factors,[36,37] cAMP (cyclic adenosine monophosphate) response element-binding protein (CREB)-binding protein (CBP) and p300,[38] and mediator subunits. In fact, PAX3-NCOA2 has two LXXLL motifs. Deguchi *et al.*[28] constructed LXXLL mutants and deletions of *MOZ-TIF2* fusion protein, and demonstrated that these abnormalities contributed to decrease anchorage-independent growth and transcriptional activity in murine bone marrow cells. On the other hand, PAX3-FOXO1A has only one LXXLL motif. Mutating it was found to decrease the transcriptional activity of FOXO1A in simian virus-40-transformed hepatocytes.[27] However the LXXLL motif did not have a key role in our experimental system using a mouse myoblast cell line transduced with human chimeric genes. This difference might be due to a difference of cell types or to a difference in the conformation of the chimeric proteins.

In conclusion, our study has two main findings: the *PAX3-NCOA2* fusion gene 1) has a dual role in the tumorigenesis of RMS, promoting cell proliferation and inhibiting myogenic differentiation and 2) is less aggressive than the *PAX3-FOXO1A* fusion gene. PAX3-NCOA2 could be a potential marker of low risk in RMS. The analyses needed to determine the risk stratification and prognostic factors of RMS have progressed from classic morphology to molecular diagnoses, using aberrant chimeric genes. The present results should help provide a more rational stratification of RMS.

MATERIALS AND METHODS

Tumor tissue samples

Tumor specimens from our patient with ERMS were surgically resected before any chemotherapy and immediately stored at − 80 °C. The patient's symptoms are described elsewhere.[13] Written informed consent was given by the parents according to the protocol approved by the institutional

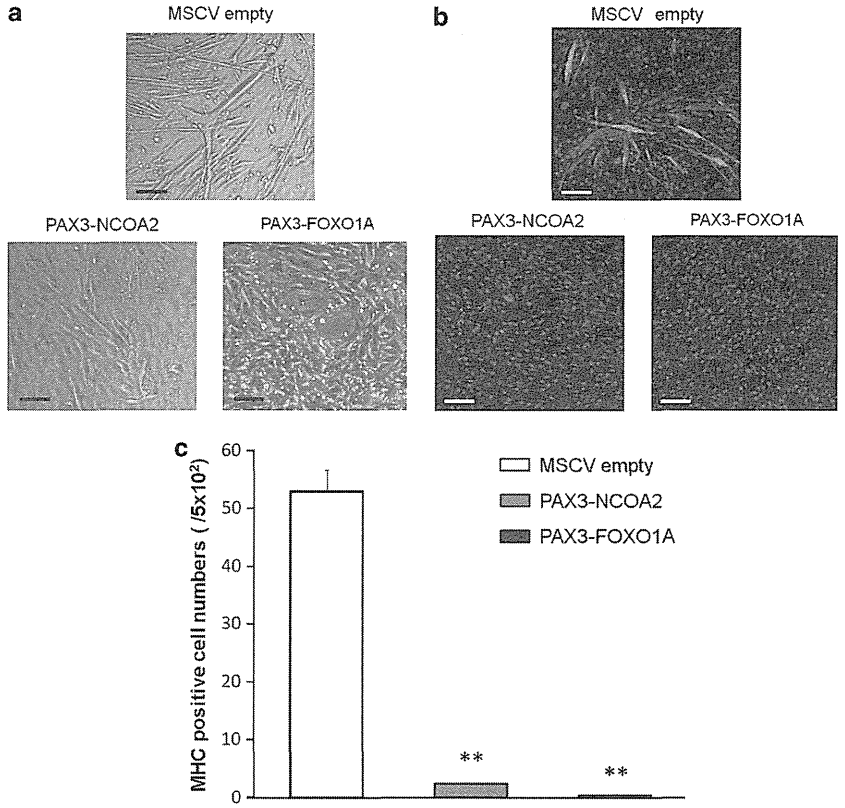

Figure 4. Inhibition of myogenic differentiation by PAX3-NCOA2 and PAX3-FOXO1A. (**a**) Representative light microscopic images of mouse myoblasts with MSCV vector alone (control), cells expressing PAX3-NCOA2 and cells expressing PAX3-FOXO1A after 4 days in differentiation medium (DM). Scale bar, 50 μm. The MSCV empty cells formed multinuclear fusion myotubes, while the PAX3-NCOA2 and PAX3-FOXO1A formed only a few fusion cells. (**b**) Fluorescent images of MHC staining after 4 days in DM. Scale bar, 100 μm. Representative images of MSCV empty showed MHC and DAPI (for nuclei), meanwhile that of PAX3-NCOA2 and PAX3-FOXO1A demonstrated few MHC-positive cells. (**c**) Numbers of MHC-positive cells per 5.0×10^2 cells. Results represent the means ± s.d. of three independent experiments. $^{**}P < 0.01$ compared with MSCV empty vector.

review board of Kyoto Prefectural University of Medicine in accordance with the Declaration of Helsinki.

FISH analysis

The BAC clones (RP11 series) were selected according to the University of California Santa Cruz Genome Browser (http://genome.ucsc.edu) and were obtained from Invitrogen (Basel, Switzerland). These BAC DNAs were isolated using a NucleoBond BAC 100 kit (Macherey-Nagel Inc., Easton, PA, USA) and were directly labeled by means of nick translation with SpectrumGreen-dUTP or SpectrumOrange-dUTP (Abbott Molecular/Vysis, Des Plaines, IL, USA). Hybridization, washing and detection were performed using standard procedures. FISH images were captured and analyzed with the PowerGene system (Applied Imaging, Santa Clara, CA, USA).

Cell cultures, transfection, infection and reagents

Mouse myoblast C2C12 cells and human embryonic kidney HEK293 were purchased from the American Type Culture Collection (Manassas, VA, USA). These cells were maintained in growth medium: Dulbecco's modified Eagle's high-glucose medium, supplemented with 10% fetal bovine serum, penicillin (100 U/ml) and streptomycin (10 mg/ml) at 37 °C in a humidified atmosphere of 5% CO_2. Stable C2C12 cell lines expressing PAX3-NCOA2, and PAX3-FOXO1A were established using a murine stem cell virus (MSCV) retrovirus expression system (Clontech Laboratories Inc., Madison, WI, USA). C2C12 cells were transfected in 60-mm dishes at ~50% confluence with 1 μg of purified expression vector DNA, 8 μl of Enhancer and 7.5 μl of Effectene (Qiagen, Hombrechtikon, Switzerland) in 1 ml of Dulbecco's modified Eagle's high-glucose medium. After 48 h, the cells were trypsinized and replanted at a 1: 5 dilution in medium. Selection of stability transfected cells was performed with 1000 μg/ml of G418 sulfate (Life Technologies, Carlsbad, CA, USA).

Reverse transcription–polymerase chain reaction (RT–PCR) and direct sequencing of PAX3-NCOA2

Total RNA was extracted from a tumor specimen with the use of an RNeasy mini kit (Qiagen) according to the manufacturer's instructions. Complementary DNA (cDNA) was synthesized with the use of the SuperScript First-Strand Synthesis System for RT–PCR (Invitrogen) according to the manufacturer's instructions. The fusion region of *PAX3-NCOA2* was PCR amplified in overlapping fragments. The primer pairs used in this experiment are listed in Supplementary Table 2. The entire coding region of PAX3-NCOA2 was PCR amplified. PCR products were sequenced with the use of the BigDye Terminator v3.1 Cycle Sequencing kit (Applied Biosystems, Rotkreuz, Switzerland) and the ABI PRISM 377 Sequence Detection System (Applied Biosystems).

Localization assay

HEK293 cells were transfected with GFP (green fluorescent protein)-PAX3-NCOA2 expression vector and the fusion protein was observed with confocal microscopy BZ-8000 (KEYENCE, Osaka, Japan).

Assay for cell proliferation

C2C12 cell lines expressing each gene or MSCV vector alone were seeded at 2×10^4 cells/well. Every 24 h, an aliquot of the cells was lysed under hypotonic conditions, and nuclei were counted with a Coulter counter (ERMA Inc., Jacksonville, FL, USA) until 96 h later (day 4).

Cell cycle analysis

Cells were plated for 72 h and then washed twice with 1 × PBS and then incubated for 30 min with propidium iodide (PI) to stain DNA. Propidium

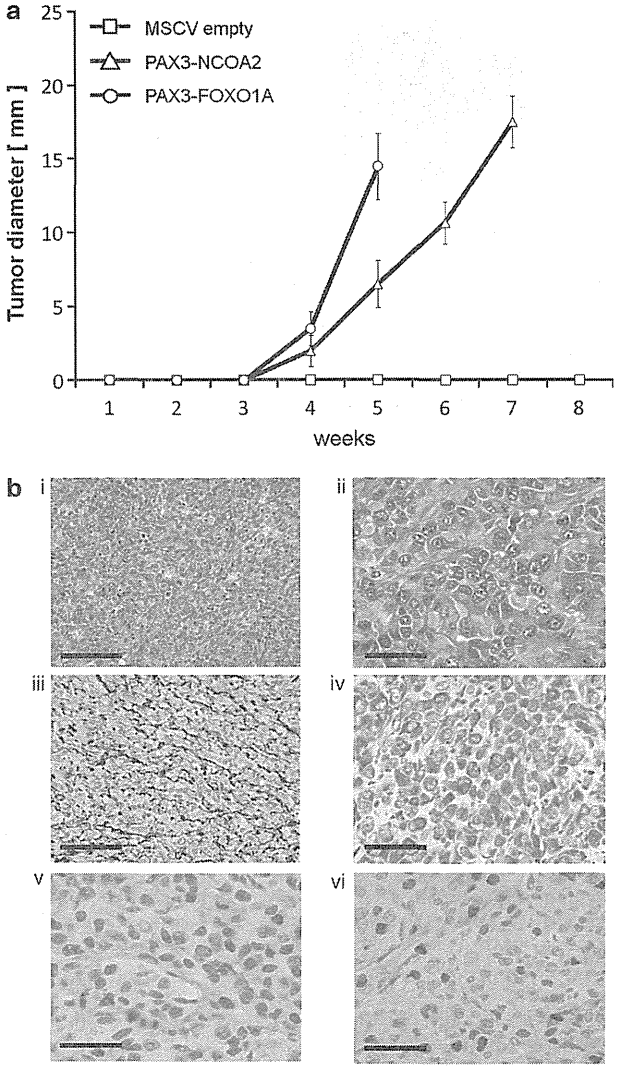

Figure 5. Effects of PAX3-NCOA2 and PAX3-FOXO1A on the proliferation of C2C12 cells in a murine xenograft model. (**a**) C2C12 cell were injected into subcutaneous tissue of BALB/c nude mice. Tumor diameters were measured every 2 or 3 days. Each point represents the means ± s.d. of three independent experiments. (**b**) Images representative of tissue sections of PAX3-NCOA2 stained with H&E (i, ii), silver impregnation (iii) and with antibodies specific for desmin (iv), myoD1 (v) and myogenin (vi). Scale bar, 200 μm (i, iii) and 100 μm (ii, iv–vi), respectively. The tumor cells ranged from small round cells to large elongated poorly differentiated cells, and exhibited varying degrees of myogenic differentiation. There were small oval or long spindle-shaped differentiated rhabdomyoblasts with eosinophilic cytoplasm, without cross striation. Even in silver impregnation (iii), there was no alveolar architecture. Also lacking was the classic cystic pattern with tumor cells palisaded against fibrovascular stroma. None of the cells were anaplastic. In the immunohistology, desmin, myoD1 and myogenin were positive; however, the expressions of myoD1 and myogenin were different. Thus, the latter differentiation in rhabdomyogenesis appeared to be abnormal or suppressed.

iodide fluorescence was read on a FACS Calibur (BD Biosciences, Franklin Lakes, NJ, USA), and the data were analyzed with Cell Quest software (BD Biosciences). The cell cycle phase was determined on the basis of DNA content using the ModFit LT Software (Verity Software House, Topsham, ME, USA) as described previously.[39]

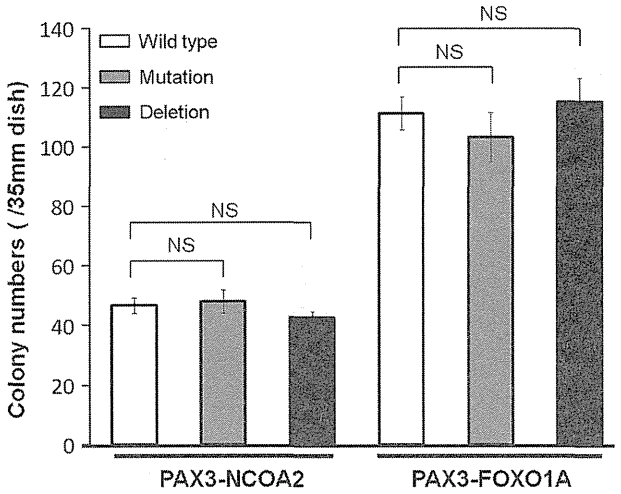

Figure 6. Effect of mutations and deletions of the LXXLL motif on anchorage-independent growth of PAX3-NCOA2 and PAX3-FOXO1A cells using a colony-forming soft agar assay. Results represent the means ± s.d. of three independent experiments. A *P*-value of less than 0.05 was considered statistically significant; NS, no significance.

Anchorage-independent soft agar colony formation assay

Cells were cultured in a two-layer soft agar system developed by Hambruger *et al.*[40] It consisted of a 1% Noble agar underlayer and a 0.7% Noble agar overlayer containing 2×10^4 cells in 35-mm dishes. Colonies were allowed to form for duration of 2 weeks with fresh media added every 3 days. Plates were stained with crystal violet and colonies more than 0.1 mm in diameter were counted.

Luciferase reporter assay for PAX3-FOXO1A enhancer

A luciferase reporter construct was generated by inserting multimerized PAX3 DNA-binding sites (6 × e5 DNA-binding sites) into pGL3 vector. A total of 1×10^5 HEK293 cells were plated per 35-mm plate and cotransfected 24 h later with FLAG expression vectors, pGL3 basic 6 × e5 vector and pRL-TK vector; 290, 90 and 20 μg, respectively. Luciferase activity was determined by using a dual luciferase assay system (Promega, Wallisellen, Switzerland) to adjust for differences in transfection efficiency. Data shows luciferase expression relative to pFLAG wild-type PAX3.

Western blot

Cells were lysed with Laemmli sample buffer. Protein concentrations in the cell lysates were measured with the Bio-Rad DC Protein Assay (Bio-Rad Laboratories, Hercules, CA, USA). Samples were boiled for 5 min in sample buffer containing bromophenol blue and 1 × β-ME, and equal amounts of protein were separated by sodium dodecylsulfate–polyaclylamide gel electrophoresis (SDS–PAGE). Electrophoretic separation was carried out on 10% polyacrylamide gel (Bio-Rad Laboratories), and the proteins were subsequently transferred to an Immobilon-P membrane (Millipore, Billerica, MA, USA). Membranes were blocked in PBST (phosphate-buffered saline with Tween 20) with 5% non-fat dry milk powder and incubated with the following primary antibodies: FLAG (Sigma-Aldrich, St Louis, MO, USA). The membranes were then washed with PBST and incubated with goat anti-mouse secondary antibody (GE Healthcare, Little Chalfont, UK) or anti-rabbit (GE Healthcare). Antibody binding was detected with the enhanced chemiluminescence detection system (ECL and ECL plus; GE Healthcare).

Assays for the differentiation of myoblast and immunofluorescence

To initiate myogenesis, cells were rinsed thoroughly with phosphate-buffered saline (PBS) before adding differentiation medium; Dulbecco's modified Eagle's high-glucose medium containing 2% Horse serum, penicillin (100 U/ml), and streptomycin (10 mg/ml) 24 h after seeding (day 1). Differentiated cells were observed on day 4 with a confocal microscope BZ-8000 (KEYENCE) to assess morphological change. For immunofluorescence, cells on cover slips were fixed with absolute

methanol, washed and incubated with anti-myosin heavy chain antibody (Sigma-Aldrich) for 1 h, rinsed with PBS, incubated with fluorescein isothiocyanate-conjugated anti-mouse IgG (Invitrogen) for 1 h, and visualized using a fluorescence microscope as previously described.[41]

Wound-healing assay

The cell layers were scratched using a pipette tip, and then cultured in the differentiation medium. Immediately after scratching (0 h), the plates were photographed and the distance between the edges of the wound area was measured and defined as 100%. At 6 h after scratching, the plates were photographed and the distance between the edges of the wound region was again measured and presented as a percentage of the distance between the edges of wound area at 0 h.

In vivo tumorigenesis

Tumors were induced in 4- to 6-week-old male athymic nude mice (BALB/c nu/nu; SHIMIZU Laboratory Supplies, Kyoto, Japan). Each mouse was injected subcutaneously with 2×10^6 C2C12 cells suspended in 0.5 ml of PBS at a single site to the lower flank. Tumor diameter was monitored every 2 or 3 days on onset of tumor formation. Mice were killed when the tumor size reached 17 mm in diameter. At the end point of the experiments, tumors were extracted and immediately photographed. A portion of the tumor was embedded in paraffin for histopathological and immunohistochemical analyses. At least three mice were used in each experiment. The mice used for this study were handled in strict adherence with local governmental and institutional animal care regulation.

Histopathology and immunohistochemistry

Histological specimens were fixed in 10% formalin and routinely processed for embedding in paraffin. Histological sections 4-μm-thick were stained with hematoxylin and eosin (H&E), silver impregnation or hybridized to antibodies specific for desmine, myoD1 and myogenin. Slides were reviewed by a board-certified pathologist (H Hojo) to define the histologic type of cancer. The sections were incubated with anti-desmin, anti-myoD1 and anti-myogenin antibody that was diluted at 1:20, 1:25 and 1:50 respectively. Sections were then treated with a VECTASTAIN Elite ABC kit (Vector Laboratories, Burlingame, CA, USA).

Mutant and deletion construction

The LXXLL motif of NCOA2 was mutagenized by inverse PCR using Topo-PAX3-NCOA2-vector with *Xho*I and *Bam* HI tags as a template. The PCRs were initiated with a 2-min incubation at 95 °C followed by 10 cycles of 95 °C for 30 s, 60 °C for 30 s and 72 °C for 7 min, and finally 10 min incubation at 72 °C. The template plasmid was digested with *Dpn* I for 1 h at 37 °C, and the remaining PCR products were treated with restriction enzymes *Xho*I and *Bam* HI. A total of 7.5 μl MSCV vector and insert DNA with 7.5 μl Ligation high ver.2 were ligated with a DNA Ligation Kit Ligation high Ver.2 (Toyobo, Osaka, Japan) according to the manufacturer's instructions. Thereafter, the composed plasmid was transformed into competent cells, and MSCV vector containing these cDNAs was generated by transfecting C2C12 cells. Mutagenesis/deletion of the LXXLL motifs of PAX3-NCOA2 and PAX3-FOXO1A were performed in the same way. The primer pairs used in this study are listed in Supplementary Table 2.

Statistical analysis

Statistical analysis was performed using the unpaired Student's *t*-test. A *P*-value of less than 0.05 was considered statistically significant.

ABBREVIATIONS

ARMS, alveolar rhabdomyosarcoma; BAC, bacterial artificial chromosome; bHLH, sequence similarity with basic helix–loop–helix motifs; CBP, CREB-binding protein; cDNA, complementary DNA; CID, CBP interaction domain; CREB, cAMP (cyclic adenosine monophosphate) response element-binding protein; DM, differentiation medium; ERMS, embryonal rhabdomyosarcoma; FISH, fluorescence *in situ* hybridization; FKHR, forkhead in human rhabdomyosarcoma; FOXO1A, forkhead box O1A; G1, Gap1; GFP, green fluorescent protein; H&E, hematoxylin and eosin; LXD, LXXLL-containing helical motif; MHC, myosin heavy chain; MSCV, murine stem cell virus; NCOA2, nuclear receptor coactivator 2; NID, nuclear receptor-interacting domain; PAS, sequence similarity with the Per Arndt-Sim (PAS) motifs; PAX3, paired box 3; PBS, phosphate-buffered saline; PBST, phosphate-buffered saline with Tween 20; PI, propidium iodide; RMS, rhabdomyosarcoma; RT–PCR, reverse transcription–polymerase chain reaction; SDS–PAGE, sodium dodecylsulfate–polyacrylamidegel electrophoresis; TAD, transactivation domain

CONFLICT OF INTEREST

The authors declare no conflict of interest.

ACKNOWLEDGEMENTS

This work was supported by Grant-in-aid for Scientific Research (A) 21249085, (A) 25253095, (B) 22390239, (C) 22591166, Grant-in-aid for Young Scientists (B) 24791078 and Grant-in-aid for Project for Development of Innovative Research on Cancer Therapeutics from the Ministry of Education, Culture, Sports, Science and Technology of Japan.

REFERENCES

1 Galili N, Davis RJ, Fredericks WJ, Mukhopadhyay S, Rauscher 3rd FJ, Emanuel BS *et al.* Fusion of a fork head domain gene to PAX3 in the solid tumour alveolar rhabdomyosarcoma. *Nat Genet* 1993; **5**: 230–235.
2 Sorensen PH, Lynch JC, Qualman SJ, Tirabosco R, Lim JF, Maurer HM *et al.* PAX3-FKHR and PAX7- FKHR gene fusions are prognostic indicators in alveolar rhabdomyosarcoma: a report from the Children's Oncology Group. *J Clin Oncol* 2002; **20**: 2672–2679.
3 Tremblay P, Gruss P. Pax: genes for mice and men. *Pharmacol Ther* 1994; **61**: 205–226.
4 Robson EJ, He SJ, Eccles MR. A PANorama of PAX genes in cancer and development. *Nat Rev Cancer* 2006; **6**: 52–62.
5 Goulding MD, Chalepakis G, Deutsch U, Erselius JR, Gruss P. Pax-3, a novel murine DNA binding protein expressed during early neurogenesis. *EMBO J* 1991; **10**: 1135–1147.
6 Jostes B, Walther C, Gruss P. The murine paired box gene, Pax7, is expressed specifically during the development of the nervous and muscular system. *Mech Dev* 1990; **33**: 27–37.
7 Barr FG. Gene fusions involving PAX and FOX family members in alveolar rhabdomyosarcoma. *Oncogene* 2001; **20**: 5736–5746.
8 Anderson J, Ramsay A, Gould S, Pritchard-Jones K. PAX3-FKHR induces morphological change and enhances cellular proliferation and invasion in rhabdomyosarcoma. *Am J Pathol* 2001; **159**: 1089–1096.
9 Lam PY, Sublett JE, Hollenbach AD, Roussel MF. The oncogenic potential of the Pax3-FKHR fusion protein requires the Pax3 homeodomain recognition helix but not the Pax3 paired-box DNA-binding domain. *Mol Cell Biol* 1999; **19**: 594–601.
10 Bernasconi M, Remppis A, Fredericks WJ, Rauscher 3rd FJ, Schafer BW. Induction of apoptosis in rhabdomyosarcoma cells through down-regulation of PAX proteins. *Proc Natl Acad Sci USA* 1996; **93**: 13164–13169.
11 Mosquera JM, Sboner A, Zhang L, Kitabayashi N, Chen CL, Sung YS *et al.* Recurrent NCOA2 gene rearrangements in congenital/infantile spindle cell rhabdomyosarcoma. *Genes Chromosomes Cancer* 2013; **52**: 538–550.
12 Sumegi J, Streblow R, Frayer RW, Dal Cin P, Rosenberg A, Meloni-Ehrig A *et al.* Recurrent t(2;2) and t(2;8) translocations in rhabdomyosarcoma without the canonical PAX-FOXO1 fuse PAX3 to members of the nuclear receptor transcriptional coactivator family. *Genes Chromosomes Cancer* 2010; **49**: 224–236.
13 Hosoi H, Kakazu N, Konishi E, Tsuchihashi Y, Hada S, Amaya E *et al.* A novel PAX3 rearrangement in embryonal rhabdomyosarcoma. *Cancer Genet Cytogenet* 2009; **189**: 98–104.
14 Hong H, Kohli K, Trivedi A, Johnson DL, Stallcup MR. GRIP-1 a novel mouse protein that serves as transcriptional coactivator in yeast for the hormone binding domains of steroid receptrors. *Proc Natl Acad Sci USA* 1996; **93**: 4946–4952.
15 Voegel JJ, Heine MJ, Zechel C, Chambon P, Gronemeyer H. TIF2, a 160 kDa transcriptional mediator for the ligand dependent activation function AF-2 of nuclear receptors. *EMBO J* 1996; **15**: 3667–3675.
16 Voegel JJ, Heine MJ, Tini M, Vivat V, Chambon P, Gronemeyer H. The coactivator TIF2 contains three nuclear receptor-binding motifs and mediates transactivation through CBP bindingdependent and -independent pathways. *EMBO J* 1998; **17**: 507–519.
17 Chen SL, Dowhan DH, Hosking BM, Muscat GE. The steroid receptor coactivator, GRIP-1, is necessary for MEF-2C-dependent gene expression and skeletal muscle differentiation. *Genes Dev* 2000; **14**: 1209–1228.

18 Ding XF, Anderson CM, Ma H, Hong H, Uht RM, Kushner PJ *et al.* Nuclear receptor-binding sites of coactivators glucocorticoid receptor interacting protein 1 (GRIP1) and steroid receptor coactivator 1 (SRC-1): multiple motifs with different binding specificities. *Mol Endocrinol* 1998; **12**: 302–313.
19 Berrevoets CA, Doesburg P, Steketee K, Trapman J, Brinkmann AO. Functional interactions of the AF-2 activation domain core region of the human androgen receptor with the amino-terminal domain and with the transcriptional coactivator TIF2 (transcriptional intermediary factor2). *Mol Endocrinol* 1998; **12**: 1172–1183.
20 Ma H, Hong H, Huang SM, Irvine RA, Webb P, Kushner PJ *et al.* Multiple signal input and output domains of the 160-kilodalton nuclear receptor coactivator proteins. *Mol Cell Biol* 1999; **19**: 6164–6173.
21 Chen D, Ma H, Hong H, Koh SS, Huang SM, Schurter BT *et al.* Regulation of transcription by a protein methyltransferase. *Science* 1999; **284**: 2174–2177.
22 Chen D, Huang SM, Stallcup MR. Synergistic, p160 coactivatordependent enhancement of estrogen receptor function by CARM1 and p300. *J Biol Chem* 2000; **275**: 40810–40816.
23 Teyssier C, Chen D, Stallcup MR. Requirement for multiple domains of the protein arginine methyltransferase CARM1 in its transcriptional coactivator function. *J Biol Chem* 2002; **277**: 46066–46072.
24 Lee YH, Coonrod SA, Kraus WL, Jelinek MA, Stallcup MR. Regulation of coactivator complex assembly and function by protein arginine methylation and demethylimination. *Proc Natl Acad Sci USA* 2005; **102**: 3611–3616.
25 Heery DM, Kalkhoven E, Hoare S, Parker MG. A signature motif in transcriptional co-activators mediates binding to nuclear receptors. *Nature* 1997; **387**: 733–736.
26 McInerney EM, Rose DW, Flynn SE, Westin S, Mullen TM, Krones A *et al.* Determinants of coactivator LXXLL motif specificity in nuclear receptor transcriptional activation. *Genes Dev* 1998; **21**: 3357–3368.
27 Nakae J, Cao Y, Daitoku H, Fukamizu A, Ogawa W, Yano Y *et al.* The LXXLL motif of murine forkhead transcription factor FoxO1 mediates Sirt1-dependent transcriptional activity. *J Clin Invest* 2006; **116**: 2473–2483.
28 Deguchi K, Ayton PM, Carapeti M, Kutok JL, Snyder CS, Williams IR *et al.* MOZ-TIF2-induced acute myeloid leukemia requires the MOZ nucleosome binding motif and TIF2-mediated recruitment of CBP. *Cancer Cell* 2003; **3**: 259–271.
29 Calhabeu F, Hayashi S, Morgan JE, Relaix F, Zammit PS. Alveolar rhabdomyosarcoma-associated proteins PAX3/FOXO1A and PAX7/FOXO1A suppress the transcriptional activity of MyoD-target genes in muscle stem cells. *Oncogene* 2013; **32**: 651–662.
30 Jothi M, Nishijo K, Keller C, AKT Mal AK. and PAX3-FKHR cooperation enforces myogenic differentiation blockade in alveolar rhabdomyosarcoma cell. *Cell Cycle* 2012; **11**: 895–908.
31 Kikuchi K, Tsuchiya K, Otabe O, Gotoh T, Tamura S, Katsumi Y *et al.* Effects of PAX3-FKHR on malignant phenotypes in alveolar rhabdomyosarcoma. *Biochem Biophys Res Commun* 2008; **365**: 568–574.
32 Finckenstein FG, Shahbazian V, Davicioni E, Ren YX, Anderson MJ. PAX-FKHR function as pangenes by simultaneously inducing and inhibiting myogenesis. *Oncogene* 2008; **27**: 2004–2014.
33 Zhang Y, Schwartz J, Wang C. Comparative analysis of paired- and homeodomain-specific roles in PAX3-FKHR oncogenesis. *J Clin Exp Pathol* 2009; **2**: 370–383.
34 Wang W, Kumar P, Wang W, Epstein J, Helman L, Moore JV *et al.* Insulin-like growth factor II and PAX3-FKHR cooperate in the oncogenesis of rhabdomyosarcoma. *Cancer Res* 1998; **58**: 4426–4433.
35 Naini S, Etheridge KT, Adam SJ, Qualman SJ, Bentley RC, Counter CM *et al.* Defining the cooperative genetic changes that temporally drive alveolar rhabdomyosarcoma. *Cancer Res* 2008; **68**: 9583–9588.
36 Parker D, Rivera M, Zor T, Henion-Caude A, Radhakrishnan I, Kumar A *et al.* Role of secondary structure in discrimination between constitutive and inducible activators. *Mol Cell Biol* 1999; **19**: 5601–5607.
37 Litterst CM, Pfitzner E. An LxxLL motif in thetransactivation domain of STAT6 mediates recruitment of NCoA-1/SRC-1. *J Biol Chem* 2002; **277**: 36052–36060.
38 Torchia J, Rose DW, Inostroza J, Kamei Y, Westin S, Glass CK *et al.* The transcriptional co-activator p/CIP binds CBP and mediates nuclear-receptor function. *Nature* 1997; **387**: 677–684.
39 Livak KJ, Schmittgen TD. Analysis of relative gene expression data using real-time quantitative PCR and the 2(-DD C(T)) method. *Methods* 2001; **25**: 402–408.
40 Hamburger AW, Salmon SE, Kim MB, Trent JM, Soehnlen BJ, Alberts DS *et al.* Direct cloning of human ovarian carcinoma cells in agar. *Cancer Res* 1978; **38**: 4118–4130.
41 Tsuchiya K, Hosoi H, Misawa-Furihata A, Houghton PJ, Sugimoto T. Insulin-like growth factor-I has different effects on myogenin induction and cell cycle progression in human alveolar and embryonal rhabdomyosarcoma cells. *Int J Oncol* 2007; **31**: 41–47.

Supplementary Information accompanies this paper on the Oncogene website (http://www.nature.com/onc)

BRIEF REPORT
FN1: A Novel Fusion Partner of ALK in an Inflammatory Myofibroblastic Tumor

Kazutaka Ouchi, MD,[1] Mitsuru Miyachi, MD, PhD,[1] Yusuke Tsuma, MD,[1] Kunihiko Tsuchiya, MD, PhD,[1] Tomoko Iehara, MD, PhD,[1] Eiichi Konishi, MD, PhD,[2] Akio Yanagisawa, MD, PhD,[2] and Hajime Hosoi, MD, PhD[1]*

Inflammatory myofibroblastic tumors (IMTs) are rare tumors characterized as low-to-intermediate grade sarcomas. Rearrangements of the anaplastic lymphoma kinase (*ALK*) gene have been reported in IMT. Here, we describe a novel fusion gene in an IMT tumor specimen. A 12-year-old male was admitted to our hospital with a bladder tumor. We identified the fibronectin 1 gene (*FN1*) as a fusion partner of *ALK* using 5′RACE. This novel fusion, *FN1–ALK*, resulted in ALK overexpression in the IMT. This finding should clarify the causes of IMT and facilitate development of novel therapeutics. Pediatr Blood Cancer © 2015 Wiley Periodicals, Inc.

Key words: ALK gene fusion; FN1; inflammatory myofibroblastic tumor

INTRODUCTION

The term "inflammatory myofibroblastic tumor (IMT)" was first introduced in 1990 in a report on 20 inflammatory pseudotumors of the lung [1]. Subsequently, IMT has been used to describe similar lesions sometimes encountered in the bladders of children [2].

Approximately half of IMTs carry rearrangements of the anaplastic lymphoma kinase (*ALK*) gene [3]. ALK is a tyrosine kinase receptor that is normally expressed in the central nervous system. Fusion of the *ALK* gene with partners such as *CLTC*, *RANBP2*, *TPM3*, *TPM4*, *CARS*, *ATIC*, *SEC1L1*, *ALO17*, and *PPFIBP* [4,5] can cause ALK overexpression and activation of the ALK kinase domain. Identification of ALK fusion genes is useful for the diagnosis of IMT and for deciding on a treatment plan, such as whether to administer an ALK inhibitor. Here, we describe a novel fusion gene encoding an oncokinase in an IMT tumor specimen.

Case Description

A 12-year-old male was admitted with a complaint of gross hematuria. Imaging studies revealed a bladder tumor. Before any therapy, the tumor was biopsied, and the specimen was flash-frozen in liquid nitrogen and stored at −80°C. Histological examination revealed a fascicular proliferation of pale basophilic spindle cells with enlarged nuclei, admixed with abundant capillaries, lymphocytes, and eosinophils. Immunohistochemical analysis revealed positive staining for ALK and α-smooth muscle actin, and negative staining for desmin (Fig. 1). FISH analysis revealed disruption of the *ALK* gene in a specimen of the bladder tumor (Supplemental Figure S1). Based on these data, we diagnosed the tumor as IMT. Neoadjuvant treatment with meloxicam (a cyclooxygenase-2 [COX2] inhibitor) reduced the size of the tumor, allowing complete resection by partial cystectomy. The patient has remained in complete remission for a year. Written informed consent for the research use of the tumor specimen was given by the parents according to the protocol approved by the institutional review board of Kyoto Prefectural University of Medicine, in accordance with the Declaration of Helsinki.

DOI 10.1002/pbc.25424
Published online in Wiley Online Library (wileyonlinelibrary.com).

METHODS

Rapid Amplification of cDNA Ends (5′-RACE) and Sequencing

Total RNA was extracted from tumor specimens using the RNeasy kit (Qiagen, Hombrechtikon, Switzerland). cDNA for RT-PCR was synthesized using the SuperScript VILO cDNA Synthesis Kit (Invitrogen, Basel, Switzerland). One microgram of total RNA was reverse-transcribed to cDNA, followed by 5′-RACE using the 5′-Full RACE Core set (Takara Bio, Shiga, Japan). The primer pairs used in this study are listed in Supplemental Table SI. Amplified products following the second PCR were cloned using the TOPO TA Cloning Kit for Sequencing (Invitrogen). The constructed plasmid DNA was sequenced using the BigDye Terminator v3.1 Cycle Sequencing kit (Applied Biosystems, Rotkreuz, Switzerland) and an ABI PRISM 3130 Sequence Detection System (Applied Biosystems).

RT-PCR

The *FN1–ALK* fusion transcript was detected by PCR using Ex Taq DNA Polymerase, Hot-Start Version (Takara Bio). PCR conditions were as follows: denaturation at 95°C for 30 sec; 30 cycles of PCR denaturation at 95°C for 30 sec, annealing at 60°C for 30 sec, and extension at 72°C for 60 sec; and a final extension at 72°C for 7 min. The PCR products were analyzed by electrophoresis

Additional Supporting Information may be found in the online version of this article at the publisher's web-site

[1]Department of Pediatrics, Graduate School of Medical Science, Kyoto Prefectural University of Medicine, Kyoto, Japan; [2]Department of Pathology, Kyoto Prefectural University of Medicine, Kyoto, Japan

Grant sponsor: JSPS KAKENHI; Grant number: (A) 25253095; Grant sponsor: Grant-in-aid of Project

Conflicts of interest: Nothing to declare.

*Correspondence to: Hajime Hosoi, Department of Pediatrics, Kyoto Prefectural University of Medicine, Graduate School of Medical Science, Kyoto, Japan. E-mail address: hhosoi@koto.kpu-m.ac.jp

Received 9 August 2014; Accepted 10 December 2014

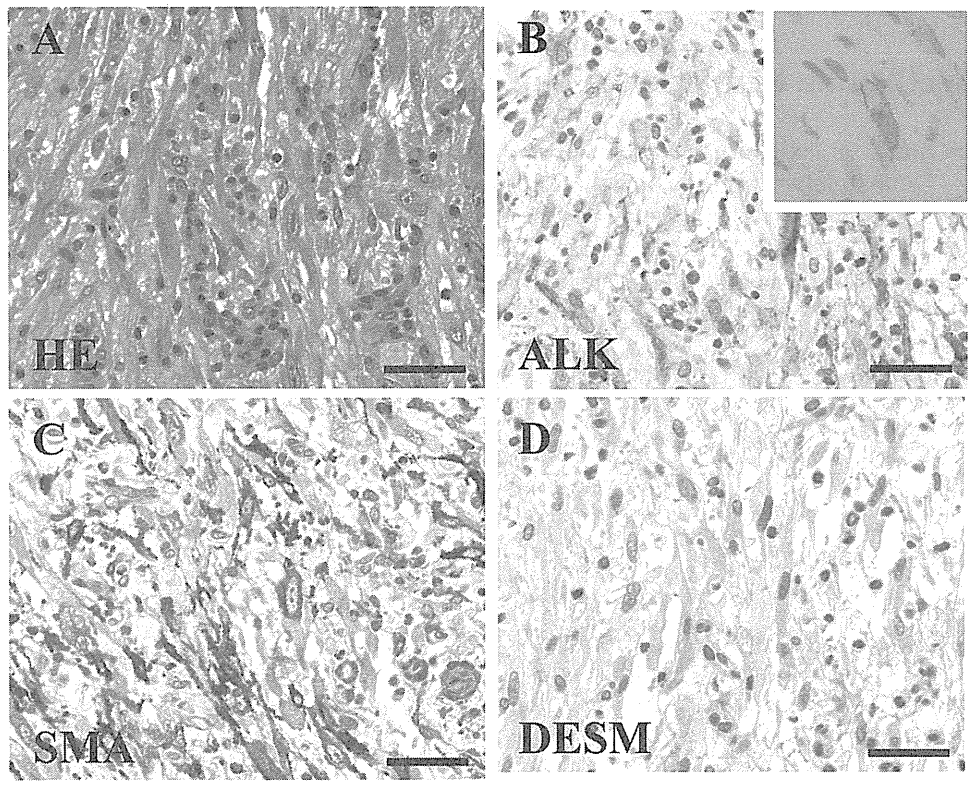

Fig. 1. Histopathological findings. Fascicular proliferation of pale basophilic spindle cells with enlarged nuclei (**A**). Tumor cells were positive for ALK (**B**) and α-smooth muscle actin (**C**), but negative for desmin (**D**). Scale bar = 5 μm.

on a 3.0% agarose gel. As an internal control for the intactness of the RNA, cDNA of the *glyceraldehyde-3- phosphate dehydrogenase (GAPDH)* gene was also amplified. The primer pairs used in this study are also listed in Supplemental Table SI.

ALK Expression Level

Total RNAs were extracted from the tumor specimen, an *NPM1–ALK*-positive anaplastic large cell lymphoma cell line (SU-HDL-1), an *EML4–ALK*-positive non-small cell lung adenocarcinoma cell line (NCI-H2228), three neuroblastoma cell lines (RTBM1, IMR32, and SH-SY5Y), and three rhabdomyosarcoma cell lines (RM2, RD, and Rh30). The neuroblastoma cell lines RTBM1 and SH-SY5Y have a cancer-associated mutation in *ALK* (F1174L) [6]. None of the rhabdomyosarcoma cell lines had *ALK* gene amplifications. Total RNAs of normal human tissues were purchased from Invitrogen. cDNAs were synthesized as described above. Real-time RT-PCR was carried out in a 7500 Fast Real-Time PCR system (Applied Biosystems) with SYBR Premix Ex Taq II (Takara Bio). Relative *ALK* mRNA expression was initially determined by ΔCt method [$2^{-(\Delta Ct)}$, where ΔCt = Ct (*ALK*) − Ct (*GAPDH*)]. This value was further normalized to the level of *ALK* mRNA in normal human brain tissue. The relevant primers are shown in Supplemental Table SI.

RESULTS

We identified a potential *ALK* fusion partner by 5′ RACE. PCR amplification of the 5′ end of *ALK* transcripts gave a 1300-bp product. The sequence of the product revealed that exon 20 of *FN1* was fused in-frame to exon 19 of *ALK* (Fig. 2). To confirm the existence of the *FN1–ALK* fusion transcript, we tested for its presence in cDNA from the IMT specimen using the *FN1* and *ALK* primers, and obtained the expected 247-bp fragment (Supplemental Figure S2).

The *ALK* expression level was higher in the tumor specimen than in other ALK fusion–positive cell lines, pediatric malignant tumor cell lines, and normal tissues (Supplemental Figure S3), suggesting that the *FN1–ALK* rearrangement results in overexpression of *ALK*.

DISCUSSION

Our results indicate the existence of a novel fusion gene, *FN1–ALK*, in an IMT. *ALK* maps to 2p23, whereas *FN1* maps to chromosome 2q34 and encodes fibronectin, which is ubiquitously expressed in many cell types and is present in dimeric or multimeric form in the extracellular matrix [7]. Ren et al. discovered the same *ALK* gene translocation, *FN1–ALK*, in an ovary stromal sarcoma patient [8]. They demonstrated that 3T3 fibroblasts overexpressing FN1–ALK generated subcutaneous tumors in nude mice, suggesting that the fusion gene had strong oncogenic potential. As in most other ALK fusion genes, the oncogenic activity of the fusion gene is probably a result of constitutive activation of ALK due to homodimerization of the fusion protein through the FN1 domain. Furthermore, because FN1 is ubiquitously abundantly expressed in human cells, the oncogenicity of the fusion could be due to high-level expression of ALK under the control of the strong FN1 promoter, as revealed by quantitative RT-PCR (Supplemental

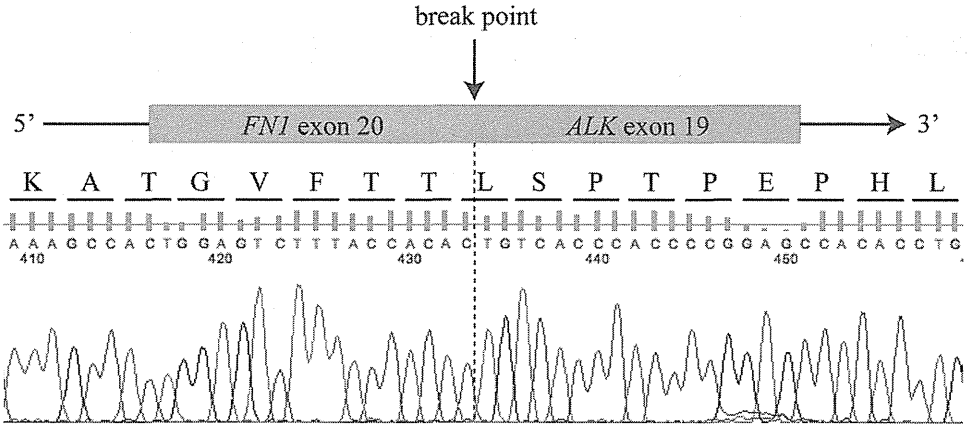

Figure 2. Novel fusion partners in IMT. Partial cDNA sequence of *FN1–ALK* showing the fusion of *FN1* exon 20 with *ALK* exon 19.

Figure S3). Unlike previously reported ALK-related fusion genes, *FN1–ALK* retains the transmembrane domain of ALK itself, encoded by exons 19–20. Retention of this domain may lead to membrane/cytoplasmic localization of ALK, which is evident from immunostaining of the tumor sample (Fig. 1).

Ren et al. also showed that ALK inhibitors dramatically suppressed the growth of 3T3 FN1–ALK tumors. Given the sensitivity of 3T3/FN1–ALK tumors to ALK inhibitors and the recent promising results obtained with crizotinib (an APT-competitive inhibitor of ALK)[9], we predict that IMT patients carrying FN1–ALK should respond well to therapy targeted against ALK.

In summary, we identified a novel fusion gene, *FN1-ALK*, in an IMT of the bladder. This discovery broadens the scope of ALK fusion oncoproteins in human cancer and identifies a potential therapeutic target for IMT.

ACKNOWLEDGMENTS

This work was supported by JSPS KAKENHI Grant Number (A) 25253095 and a Grant-in-aid of Project for Development of Innovative Research on Cancer Therapeutics (P-Direct) from the Ministry of Education, Culture, Sports, Science, and Technology of Japan.

REFERENCES

1. Pettinato G, Manivel JC, De Rosa N, Dehner LP. Inflammatory myofibroblastic tumor (plasma cell granuloma). Clinicopathologic study of 20 cases with immunohistochemical and ultrastructural observations. Am J Clin Pathol 1990;94:538–546.
2. Netto JM, Perez LM, Kelly DR, Joseph DB. Pediatric inflammatory bladder tumors: Myofibroblastic and eosinophilic subtypes. J Urol 1999;162:1424–1429.
3. Coffin CM, Patel A, Perkins S, Elenitoba-Johnson KS, Perlman E, Griffin CA. ALK1 and p80 expression and chromosomal rearrangements involving 2p23 in inflammatory myofibroblastic tumor. Mod Pathol 2001;14:569–576.
4. Takeuchi K, Soda M, Togashi Y, Sugawara E, Hatano S, Asaka R, Okumura S, Nakagawa K, Mano H, Ishikawa Y. Pulmonary inflammatory myofibroblastic tumor expressing a novel fusion, PPFIBP1-ALK: Reappraisal of anti-ALK immunohistochemistry as a tool for novel ALK fusion identification. Clin Cancer Rese 2011;17:3341–3348.
5. Cools J, Wlodarska I, Somers R, Mentens N, Pedeutour F, Maes B, De Wolf-Peeters C, Pauwels P, Hagemeijer A, Marynen P. Identification of novel fusion partners of ALK, the anaplastic lymphoma kinase, in anaplastic large-cell lymphoma and inflammatory myofibroblastic tumor. Genes Chromosomes Cancer 2002;34:354–362.
6. Hallberg B, Palmer RH. Mechanistic insight into ALK receptor tyrosine kinase in human cancer biology. Nature Rev Cancer 2013;13:685–700.
7. Mao Y, Schwarzbauer JE. Fibronectin fibrillogenesis, a cell-mediated matrix assembly process. Matrix Biol 2005;24:389–399.
8. Ren H, Tan ZP, Zhu X, Crosby K, Haack H, Ren JM, Beausoleil S, Moritz A, Innocenti G, Rush J, Zhang Y, Zhou XM, Gu TL, Yang YF, Comb MJ. Identification of anaplastic lymphoma kinase as a potential therapeutic target in ovarian cancer. Cancer Res 2012;72:3312–3323.
9. Butrynski JE, D'Adamo DR, Hornick JL, Dal Cin P, Antonescu CR, Jhanwar SC, Ladanyi M, Capelletti M, Rodig SJ, Ramaiya N, Kwak EL, Clark JW, Wilner KD, Christensen JG, Janne PA, Maki RG, Demetri GD, Shapiro GI. Crizotinib in ALK-rearranged inflammatory myofibroblastic tumor. N Engl J Med 2010;363:1727–1733.

日本神経芽腫研究グループ（JNBSG）規約（第４版）

日本神経芽腫研究グループ（JNBSG）規約
第１版　2006年 5月 26日　運営委員会承認
第２版　2006年 9月 1日　運営委員会承認
第３版　2007年 11月 23日　運営委員会承認
第４版　2008年 5月 10日　運営委員会承認

第１章　総　則

（名称）
第１条
本会の名称は日本神経芽腫研究グループ（Japan Neuroblastoma Study Group, JNBSG）とする.

（目的）
第２条
JNBSGは神経芽腫の基礎的・臨床的研究を行い，治療成績と患者の生活の質の向上をはかり，神経芽腫患者の健康と福祉に貢献することを目的とする.

（活動）
第３条
JNBSGは前条の目的を達成するために次の活動を行う.
1) 質の高い臨床試験に基づいた神経芽腫の治療研究.
2) 神経芽腫の診断および病態解明に関する基礎的・臨床的研究.
3) 国内および国外の関係諸団体との情報交換および協力活動.
4) その他，目的を達成するために必要な活動.

（会員）
第４条
JNBSGは一般会員および名誉会員により構成される.（細則参照）

（参加施設）
第５条
JNBSGの参加施設はJNBSG施設ならびにJNBSG協力施設とする. JNBSG施設は治療を担当する医療機関とし，JNBSG協力施設は研究機関ならびにJNBSGの活動を支援する医療または研究機関とする.（細則参照）

（役員）
第６条
JNBSGには以下の役員をおく.（細則参照）
1) 会長　１名
2) 副会長　１名
3) 幹事　６名（副会長１名を含む）
4) 運営委員長　１名
5) 運営委員　２０－３０名

6) 監事　　2名
7) データセンター長　1名
8) 検体センター長　　1名
9) 事務局長　　1名

（役員の役割）
第7条
1．会長はJNBSGを代表し，幹事会および運営委員会を招集する．幹事会では議長を担当する．
2．副会長は会長を補佐する．
3．幹事は運営委員会に対し，JNBSG活動の企画・立案を含めた必要な助言を行う．
4．運営委員長は運営委員会の議長として運営委員会の取りまとめを行う．
5．運営委員は運営委員会を構成し，JNBSGの活動を審議し，実行する．
6．監事は運営委員会の審議を含むJNBSG活動の全般を監査する．
7．データセンター長はデータセンター業務の取りまとめを行う．
8．検体センター長は検体センター業務の取りまとめを行う．
9．事務局長は事務局業務の取りまとめを行う．

（組織・機能）
第8条
1．JNBSGは幹事会，運営委員会の他，JNBSG活動の遂行とその円滑な運営を目的に，各種委員会ならびにデータセンター，検体センターおよび事務局を設置する．（細則参照）
2．幹事会は会長，副会長，幹事および運営委員長で構成し，JNBSG活動の基本的方針を検討・提言する．
3．運営委員会は会長，副会長，幹事，運営委員長，運営委員，各委員会委員長，データセンター長，検体センター長，監事および事務局長によって構成し，JNBSG活動を審議・決定し，これを実行する．各種委員会は運営委員会内に設置し，運営委員は委員会の委員長を兼務することができる．
4．データセンターはJNBSG症例の登録・管理を行い、臨床研究（試験）のデータ管理と機能的中心としての役割を担当する．ただし後者は運営委員会が必要と判断したものに限定される．
5．検体センターは臨床研究（試験）にともなう中央診断・検体管理を主たる業務とし，これを担当する．
6．事務局は会員管理，総会・幹事会・運営委員会　等の開催，会計などを含む事務局業務を担当する．

（幹事会，運営委員会，総会および研究会の召集と議決）
第9条
1．会長は幹事会および運営委員会を年に1回以上，召集し開催する．会の成立には過半数の出席を要し，案件の議決には議決権を有する出席者の過半数の賛成を要する．監事は運営委員会の議決権を有さない．
2．会長はJNBSGの目的を達成するために年に1回以上，総会および研究会を招集・開催し，JNBSG活動に関する情報を会員に公開・周知するとともに会員の意見を広く収集しJNBSG活動に反映する．

（入会および退会）
第10条
1．JNBSGに会員または参加施設として入会を希望する医師・研究者または医療機関・研究機

関は会長に入会を申請し，幹事会の承認を得る．
２．運営委員は会員または参加施設を会長に推薦することができる．
３．退会を希望する会員または参加施設は会長に退会を申請し，幹事会の承認を得る．
４．JNBSG の会員または参加施設が不適格と判断された場合には，会長は幹事会の承認を得た上で会員または参加施設を退会させることができる．

（規約の変更）
第１１条
本規約を変更する場合は運営委員会の議決を経て幹事会の承認を得る．会長，幹事および運営委員は規約の変更を発議することができる．

（細則）
第１２条
総則を施行するために細則を設ける．細則は運営委員会の議決を経て幹事会で承認する．会長，幹事および運営委員は細則の変更を発議することができる．

（規約の発効）
第１３条
本規約は平成２０年５月１０日より発効する．

日本神経芽腫研究グループ（JNBSG）規約細則（第 11 版）

日本神経芽腫研究グループ（JNBSG）規約細則

第 1 版	2006 年 5 月 26 日	運営委員会承認
第 2 版	2006 年 9 月 1 日	運営委員会承認
第 3 版	2007 年 11 月 23 日	運営委員会承認
第 4 版	2008 年 5 月 10 日	運営委員会承認
第 5 版	2009 年 1 月 24 日	運営委員会承認
	2009 年 6 月 12 日	一部修正・承認
第 6 版	2009 年 9 月 25 日	運営委員会承認
第 7 版	2010 年 5 月 8 日	運営委員会承認
第 8 版	2012 年 1 月 27 日	運営委員会承認
第 9 版	2012 年 9 月 29 日	運営委員会承認
第 10 版	2014 年 6 月 8 日	運営委員会承認
第 11 版	2015 年 1 月 23 日	運営委員会承認

第２章　細　則

（専門委員会）

第１条

１．JNBSG は以下に定める専門委員会を運営委員会のもとに設置する．各専門委員会の委員は兼任不可とする．ただし，5）に定めるリスク分類委員会は，他の専門委員会とは異なる横断的な委員会とし，他の専門委員会委員との兼任を可とする．８）に定めるプロトコール検討委員会は、１）化学療法委員会，２）放射線治療委員会，３）外科治療委員会の全委員に必要な委員を加えた横断的委員会とし、他の専門委員会との兼任を可とする．また，細則第２条に記載する恒常委員会委員との兼任は可とする．

1）　化学療法委員会
2）　放射線療法委員会
3）　外科療法委員会
4）　中央病理診断委員会
5）　リスク分類委員会
6）　統計委員会
7）　プロトコール検討委員会
8）　ホームページ委員会
9）　研究支援委員会
10）　画像診断委員会

２．各専門委員会の委員は６名程度とするが必要に応じて増減できる．各専門委員会の委員長は幹事会が推薦し、運営委員会の承認を得る．

３．専門委員会の委員長は運営委員会の承認のもとに作業部会を組織することができる．作業部会のメンバーは各委員会における実務的な作業を行い，委員会に出席できる．

４．専門委員会の目的・業務等については委員会規約に定める．委員会は活動の円滑な遂行を目的に細則または内規を定めることができるが，いずれも運営委員会の承認を必要とする．

（恒常委員会）

第２条

1．JNBSG は以下に定める恒常委員会を設置する．恒常委員会は第三者的性格を持つ独立した委員会であるため，他の小児がんの治療研究グループと連携することができ，委員長および委員は JNBSG 会員・非会員いずれからも選定することができる．各恒常委員会は，それぞれに定めた手順によって職務を遂行する．恒常委員会委員と専門委員会委員の兼任は可とする．
   1) 倫理審査委員会
   2) 効果安全性評価委員会
   3) 外部諮問委員会
2．恒常委員会の目的・業務等については委員会規約に定める．委員会は活動の円滑な遂行を目的に細則または内規を定めることができるが，いずれも運営委員会の承認を必要とする．

（役員の選出方法および任期等）
第３条
1．会長は運営委員会で運営委員の中から別途定める手順に基づく選挙により選出する．任期は３年，連続再任は１回までとする．
2．副会長は会長が幹事の中から指名する．任期は３年，連続再任は１回までとする．会長・副会長は，委員会の委員長は兼任できない．
3．委員会の委員長は幹事会が推薦し，運営委員会の承認を得る．任期は３年，連続再任は１回までとする．委員会の委員は委員長が指名し，運営委員会の承認を得る．
4．運営委員は２０名以上３０名以内とする．任期は３年で再任を妨げない．JNBSG 会員の中から別途定める手順に基づく選挙により選出する．人数は地域性を考慮し，北海道１，東北２，関東甲信越１０，東海北陸３，近畿４，中四国２，九州３とする．会長は会の運営に必要な運営委員を別途に若干名指名することができる．
5．運営委員長は運営委員の互選にて選任する．任期は３年，連続再任は１回までとする．運営委員長は，会長，副会長，または幹事との兼任を可能とする．
6．幹事会は会長，副会長，および運営委員長を含む８名の委員から構成される．幹事は運営委員の中から運営委員の互選で選任する． 任期は３年とするが次期運営委員による初回運営委員会開催までその任を継続する。連続再任は１回までとする．
7．監事は運営委員以外の JNBSG 会員から運営委員会で選任する．監事は運営委員会に出席できるが，議決権はない．監事の任期は３年とし，連続再任を認めない．
8．データセンター長および検体センター長はそれぞれ運営委員会において承認されたデータセンターおよび検体センターから選出され，幹事会がこれを承認する．
9．事務局長は会長が任命し，幹事会がこれを承認する．
１０． 役員の任期中に退職等の理由により役員の継続が不可能となった場合は，新たな役員を置く．任期は残る期間とし，選出方法は各役員の選出方法に準ずる．

（選挙と選挙権）
第４条
1．全ての JNBSG 会員は被選挙権を有する．
2．JNBSG 施設および JNBSG 協力施設の全ての施設研究責任者は選挙権を有する．
3．何らかの事情で選挙の時期を延期せざるを得ない場合は、幹事会および運営委員会の議決を経て総会において報告する。
4．細則第３条に定める通り，会長と運営委員は別途定める手順に基づく選挙によって選出する．

（参加施設の要件および責務）
第５条

1．JNBSG 施設の要件

JNBSG 施設は以下の４項目を満たしてなければならない．

1）集学的治療ができる小児がん治療チームを有する，大学病院，専門病院またはそれに準ずる施設である．

2）施設内に機関審査委員会（IRB）あるいは倫理審査委員会がある．

3）日本小児血液・がん学会会員が常勤医として勤務している．

4）施設モニタリングおよび監査の受け入れが可能である．

2．JNBSG 施設の責務

1）JNBSG 施設は臨床研究に参加し，治療を担当する主たる医師を登録し，研究責任者及び実務担当者各１名（兼任可）を届け出る．研究責任者および実務担当者は，施設の常勤医でなければならない．

2）JNBSG 施設の研究責任者は JNBSG から伝えられた情報を施設内の会員に遅滞なく伝える．

3）JNBSG 施設の実務担当者はデータセンターの求めに応じて速やかに必要な事務的書類を提出する．

4）JNBSG 施設は積極的に JNBSG 研究に参加し，本規約を守り，継続的に症例を登録かつ追跡する．

5）JNBSG 施設はデータセンターの求めに応じて，指定の様式によって速やかにデータを報告する．

6）JNBSG 施設は別途に定める年会費を納めなければならない．なお，会費を３年間滞納した施設は自動的に JNBSG 施設の資格を失う．

7）JNBSG 施設は上記１）～５）に記載した責務に関し，年１回のパフォーマンス評価を受ける．評価スコアは運営委員会にて検討され，必要な措置が決定される．具体的な評価手順は別途定める．

3．JNBSG 協力施設の要件

JNBSG 協力施設は以下の２項目を満たしてなければならない．

1）小児がんに関する研究や研究支援の実績があると幹事会によって判断された施設であり，特に治療を担当しない国公私立の研究所，またはそれに準じた施設（同一施設に病院と研究所が併設されている場合は，病院を JNBSG 施設，研究所を JNBSG 協力施設として可）．

2）施設内に機関審査委員会（IRB）あるいは倫理審査委員会がある．

4．JNBSG 協力施設の責務

1）JNBSG 協力施設は研究責任者および実務担当者各１名（兼任は可），および当該施設に所属する研究協力者を届け出る．

2）JNBSG 協力施設の研究責任者は JNBSG から伝えられた情報を施設内の会員に遅滞なく伝える．

3）JNBSG 協力施設の実務担当者は第８条に定めるデータセンターの求めに応じて速やかに必要書類を提出する．

4）JNBSG 協力施設は本規約を守り，積極的に JNBSG 研究を支援し，継続的に活動する．

（会員の分類，要件および責務）

第６条

1．JNBSG 会員は一般会員および名誉会員とする．

2．一般会員（以下，会員）の分類と要件

1）JNBSG 会員は日本小児血液・がん学会の会員でなければならない。

2）JNBSG 施設に属する医師・研究者のうち，JNBSG 参加を申請して幹事会で承認された者を「A 会員」とする．なお、JNBSG 施設の研究責任者と実務担当者は、必ず A 会員とな

る.

3) JNBSG 協力施設に所属する医師・研究者のうち，JNBSG 参加を申請して幹事会で承認された者を「B 会員」とする．なお、JNBSG 協力施設の研究責任者と実務担当者は、必ず B 会員となる．

4) いずれの施設にも属さないが JNBSG 参加を希望し，幹事会で承認された者を「C 会員」とする．

5) JNBSG 施設において JNBSG 会員にはならないが，患者治療を担当する医師は「施設研究協力者」と定義する．

3．会員の責務

1) JNBSG 会員は，総会や関連する研究会に出席し，積極的に JNBSG 活動に参加する責務を負う．

2) JNBSG 会員は細則第 11 条に定める年会費を納めなければならない．

3) 施設研究協力者は，施設実務担当者を通して情報を得ることができ，JNBSG が主催する研究会などに参加できる．

4．名誉会員

会長または幹事会は，JNBSG に多大な貢献をした一般会員を名誉会員として運営委員会に推薦することができる．運営委員会の承認を得られた名誉会員は，運営委員会に参加することができ、また一般会員と同様に JNBSG 活動に参加できるが，会費の納入は免除される．

（事務局）

第７条

1．JNBSG 事務局は筑波大学（茨城県つくば市天王台 1－1－1 医学医療系）に置く．

2．JNBSG 事務局は JNBSG 会議の招集・開催，会員・参加施設の管理，広報，会計等の業務に関わる事務を担当する．

（データセンター）

第８条

1．データセンターは，国立成育医療研究センター研究所に置く．

2．データセンターは，以下の業務を行う．

1) 研究計画および計画書作成への参画

2) 症例登録

3) データ管理

4) 薬剤安全情報の収集

5) 臨床研究（試験）進捗状況のモニター

3．データセンターはデータ管理業務の一部を外部に委託することができる．

（検体センター）

第９条

1．検体センターは国立成育医療研究センター研究所、千葉県がんセンター研究所および埼玉県立がんセンター臨床腫瘍研究所に置く．

2．検体センターは JNBSG 施設から提出された患者由来の検体に関わる以下の業務を行う．

1) 病理組織ならびに生物学的特性の中央診断

2) 検体またはその抽出物の保存・管理と二次利用のための事務的業務

（報告および発表）

第１０条

1．委員会の委員長は委員会活動を運営委員会に報告する．
2．JNBSG 会員が JNBSG の活動によって得た学術的知見は，幹事会および運営委員会の許可を得たうえで，別途定める規約にしたがい発表することができる．発表者は発表の内容を運営委員会ならびに総会において報告する．
3．データセンターおよび検体センターは運営委員会および総会において，臨床試験と検体集積に関する進捗状況を定期的に報告する．

（運営費）
第１１条
1．JNBSG は年会費および寄付金により運営される．JNBSG 施設は別途定める年会費を支払わねばならない．必要に応じ，総会の際に会場費を徴収することができる．
2．JNBSG は会の運営に必要な資金を集めるために，公的・私的機関への研究助成の応募ならびに寄付金の募集をすることができる．
3．年会費は JNBSG 施設につき２０，０００円とする．JNBSG 会員個人の年会費は当面の間無料とする．
4．会計年度は、４月１日から翌年３月３１日までとする。

（規約の発効）
第１２条
本規約細則は平成２７年１月２３日より発効する．

Jpn J Radiol (2014) 32:529–536
DOI 10.1007/s11604-014-0340-y

ORIGINAL ARTICLE

Efficacy of preoperative transcatheter arterial chemoembolization combined with systemic chemotherapy for treatment of unresectable hepatoblastoma in children

Masakazu Hirakawa · Akihiro Nishie · Yoshiki Asayama · Nobuhiro Fujita · Kousei Ishigami · Tatsurou Tajiri · Tomoaki Taguchi · Hiroshi Honda

Received: 26 February 2014 / Accepted: 3 June 2014 / Published online: 13 June 2014

Abstract
Purpose The purpose of this study was to evaluate, retrospectively, the clinical efficacy of preoperative transcatheter arterial chemoembolization (TACE) combined with systemic chemotherapy for unresectable hepatoblastoma.
Materials and methods Five boys and three girls (mean age 15.2 months) were treated with preoperative TACE combined with systemic chemotherapy for unresectable hepatoblastomas. Mean tumor diameter and mean alfa-fetoprotein (AFP) level were 11.8 cm and 549,386 ng/mL, respectively. Pretreatment, the extent of disease (PRETEXT) was: II, 1; III, 6; IV, 1. For all patients, preoperative systemic chemotherapy was administered before TACE. At each TACE, carboplatin and adriamycin mixed with iodized oil were infused into the feeding arteries. Tumor response and prognosis after treatment were evaluated.
Results TACE resulted in few Grade 1 adverse effects (AEs), without G3 or more AEs, according to CTACAE 3.0. Mean tumor shrinkage was 60.9 %, and the mean AFP decrease from initial levels was 94.8 %. In all cases TACE combined with systemic chemotherapy enabled subsequent safe and complete surgical resection. After a mean follow-up of 59 months, tumor-free survival was 75 %.
Conclusion Preoperative TACE combined with systemic chemotherapy was effective in inducing surgical resectability of unresectable hepatoblastoma.

Keywords Hepatoblastoma · TACE · Systemic chemotherapy

Introduction

Hepatoblastoma is the most common malignancy of the liver among infants and children [1–3]. It is well known that the resectability of the primary tumor is the most

This paper was presented at an RSNA meeting in 2009.

M. Hirakawa (✉) · A. Nishie · Y. Asayama · N. Fujita · K. Ishigami · H. Honda
Department of Clinical Radiology, Graduate School of Medical Sciences, Kyushu University, 3-1-1 Maidashi, Higashi-ku, Fukuoka 812-8582, Japan
e-mail: mahira@radiol.med.kyushu-u.ac.jp

A. Nishie
e-mail: anishie@radiol.med.kyushu-u.ac.jp

Y. Asayama
e-mail: asayama@radiol.med.kyushu-u.ac.jp

N. Fujita
e-mail: n-fujita@med.kyushu-u.ac.jp

K. Ishigami
e-mail: ishigami@radiol.med.kyushu-u.ac.jp

H. Honda
e-mail: honda@radiol.med.kyushu-u.ac.jp

T. Tajiri
Department of Pediatric Surgery, Kyoto Prefectural University of Medicine, 1-5 Hangi-cho, Shimogamo, Sakyo-ku, Kyoto 606-8522, Japan
e-mail: taji@koto.kpu-m.ac.jp

T. Taguchi
Department of Pediatric Surgery, Graduate School of Medical Sciences, Kyushu University, 3-1-1 Maidashi, Higashi-ku, Fukuoka 812-8582, Japan
e-mail: taguchi@pedsurg.med.kyushu-u.ac.jp

important factor determining the long-term survival of children with hepatoblastoma, and complete surgical resection of the primary tumor is absolutely vital to achieve cure [3–10]. However, 50 % of cases are unresectable at initial presentation because of local bilobar disease, portal invasion, or metastatic spread. This situation has traditionally been associated with a poor prognosis [3, 6, 7, 11]. Preoperative systemic chemotherapy is vital to reduce tumor size and control tumor spread, to convert an unresectable tumor to a resectable one, thus improving prognosis [7]. However, the associated systemic adverse effects, for example myelosuppression and cardiotoxicity, sometimes lead to delayed surgery and hence tumor regrowth and chemotherapy-related death [12]. There are also problems of drug resistance [9], and induction of a second malignancy [13, 14] by use of anticancer drugs. To reduce these disadvantages of systemic chemotherapy, transcatheter arterial chemoembolization (TACE) may be an alternative to systemic chemotherapy. TACE has the advantages of maximum drug uptake by the tumor and minimum systemic exposure to the drug. It can, furthermore, be combined with arterial embolization, to occlude feeding arteries, and thus induce ischemic tumor necrosis and prolong the dwell time of anticancer drugs in the tumor vasculature, which enhances their effect [12]. We report a series of hepatoblastoma cases that were successfully treated by preoperative TACE combined with systemic chemotherapy. The clinical efficacy of preoperative TACE combined with systemic chemotherapy, and tumor response and prognosis, were evaluated.

Materials and methods

The retrospective study was performed with the approval of our institutional review board, and written informed consent was obtained from all the patients' legal guardians.

Patients

Between March 2001 and March 2008, 11 children with hepatoblastoma were referred to our institution. Three children underwent right lobectomy without preoperative systemic chemotherapy and TACE, because their tumors were located in the right lobe only and no invasion of the portal vein and hepatic vein was revealed by preoperative contrast-enhanced computed tomography (CT). The other eight children, treated by preoperative TACE combined with systemic chemotherapy for unresectable hepatoblastoma, form the basis of this study. The patients consisted of five boys and three girls, ranging in age from 3 to 38 months (15.2 ± 4.0 months, mean ± SD). We did not perform biopsies before treatment, because of the risk of hemorrhage and invasiveness. Diagnosis was made before treatment on the basis of hypervascular hepatic tumor on contrast-enhanced CT findings and high serum α-fetoprotein (AFP) levels. Contrast-enhanced CT was performed to evaluate the tumor site on the basis of which hepatic segments were occupied by the tumor, the pretreatment extent of disease (PRETEXT) [1], the tumor size measured by the maximum diameter on cross-sectional images, and the presence or absence of distant metastasis. The tumor was considered unresectable when there was bilobar disease or inferior vena cava invasion (case 2) before treatment. The patients' characteristics before treatment are summarized in Table 1.

All tumors were diagnosed as hepatoblastoma (1 well differentiated and 7 poorly differentiated) on the basis of pathological examination of resected specimens. Tumor diameter was 11.8 ± 1.2 cm (mean ± SD; 6–16 cm), and AFP level was 549,386 ± 216,091 ng/mL (mean ± SD). The pretreatment extent of disease (PRETEXT) was: II, 1; III, 6; IV, 1.

Treatment

The procedure used for managing cases of unresectable hepatoblastoma was as follows. Patients initially underwent systemic chemotherapy in accordance with the principles of the regimen of the Japanese Study Group for Pediatric Liver Tumor (JPLT-2) protocol [15]. The chemotherapy regimen consisted of repeated courses of cisplatin (CDDP), 80 mg/m^2 × 1 day, and tetrahydropyranyl-adriamycin (THP-ADR), 30 mg/m^2 × 2 days. These courses were repeated every 4 weeks until the tumor showed no response or poor response to systemic chemotherapy, as assessed by enhanced CT scan and serum AFP levels. When their cardiac function, renal function, liver function, and inflammatory reaction improved, patients underwent TACE, by use of the following procedure, irrespective of the resectability of the primary tumor. Under general anesthesia, the femoral artery was catheterized by use of the Seldinger technique. A 3-F or 4-F sheath (Supersheath; Medikit, Tokyo, Japan) was placed in the groin. Under fluoroscopic digital subtraction angiography (DSA), a 3-Fr or 4-Fr cobra-shaped catheter (Medikit) was manipulated into the celiac axis and superior mesenteric artery. Arteriography using 61 % iopamidol (Iopamiron 300; Bayer Japan, Tokyo, Japan) was performed to reveal the anatomy of the hepatic artery and portal vein, identify accessory arteries, and confirm the patency of the portal vein. Through the catheter, a 2.4-Fr (Sniper 2; Clinical Supply, Gifu, Japan) or 2.0-Fr (Mester Cath; Medikit) microcatheter was selectively introduced and directed to the artery supplying the tumor. First, carboplatin (200 mg/m^2) was injected into the feeding artery.